Applied Geography 187 (2026) 103893

Contents lists available at ScienceDirect

Applied Geography

journal homepage: www.elsevier.com/locate/apgeog

A multimodal framework for assessing park accessibility and equity from spatial proximity to experiential quality

Wenting Luo [a], Yuting Guo [b], Robert Tenzer [a,*], Yang Xu [a], Zhongtian Ma [a]

[a] Department of Land Surveying and Geo-Informatics, Hong Kong Polytechnic University, Hong Kong, China
[b] College of Urban and Environmental Sciences, Central China Normal University, 152 Luoyu Rd, Wuhan, PR China

ARTICLE INFO

Handling Editor: J Peng

Keywords:
Experiential quality
Green view index
Multimodal
Park accessibility

ABSTRACT

Ensuring equal access to urban parks is vital for sustainable city development. However, prevailing assessment of park accessibility, which mainly rely on spatial proximity, offer a limited perspective by overlooking destination appeal and journey quality. Utilizing social media and street view images, this study proposes a novel multimodal framework that advanced the evaluation of park accessibility from spatial proximity to experiential quality. The framework first integrated online public feedback and offline facility quality using the PCA-AHP-TOPSIS method to evaluate park attractiveness. Then a greenery-perceived distance was proposed by integrating street-level visual greenness and travel distance across three modes to model the perceived impedance of journeys. The effectiveness of the proposed framework is tested in the main area of Wuhan, China. The results reveal that the proposed attraction coefficient correlates more strongly with actual park usage ($R^2 = 0.68$) than area-based metrics ($R^2 = 0.41$). Incorporating GVI significantly improves the explanatory power for visitation frequency, particularly for walking (R^2 increase from 0.45 to 0.50) and cycling (from 0.44 to 0.48). GVI's influence varies across travel modes: within a 30-min threshold, walking visitation shows a strong positive correlation with GVI while being weakly affected by distance, whereas distance remains the dominant deterrent for cycling and driving. A pronounced spatial disparity is identified, with 45.3 % of walking zones lacking park access within 30 min, highlighting a mismatch between accessibility and population density. This framework provides practical tools for urban planning and public health, contributing meaningfully to the long-term sustainable development of cities.

1. Introduction

Urban parks are the primary recreational and leisure spaces for city residents (Chiesura, 2004), playing a crucial role in promoting both physical (McCormack et al., 2010) and mental health (Jiang et al., 2021). Beyond health benefits, urban parks function as natural cooling systems, help maintain biodiversity (Biella et al., 2025), regulate the urban climate (Doick et al., 2014), and improve air quality (Islam et al., 2024). However, with rapid urbanization and population growth, the distribution of parks has become increasingly uneven, leading to intensified competition for these valuable green resource (Chen, Li, et al., 2024). Consequently, ensuring equitable access, especially in high-demand areas, has become a critical issue in environment justice and urban planning areas (Wüstemann et al., 2017), aligning with the United Nations' Sustainable Development Goals (SDGs), particularly SDG 3 (Good Health and Well-being) and SDG 11 (Sustainable Cities and Communities) (UN, 2015). Therefore, accurately assessment of park accessibility, the ease of reaching and utilizing parks, is paramount for assessing and promoting spatial equity in green space (Hamstead et al., 2018).

Early studies primarily focused on the spatial distribution and physical accessibility of parks, using park area as the core metric for supply (Bertram & Rehdanz, 2015). Specifically, methods such as the container model, buffer analysis, and network analysis, relied exclusively on size-based thresholds to define supply capacity, as exemplified by Talen (1997) centroid-based calculations, Nicholls (2001) buffering techniques, and Comber et al. (2008) network distance approaches. However, relying solely on park size fails to capture variations in quality and attractiveness, which strongly influence residents' park use (Wu et al., 2017). To address this limitation, recent studies have begun to

* Corresponding author.
E-mail addresses: Wenting.luo@connect.polyu.hk (W. Luo), ytguo@mails.ccnu.edu.cn (Y. Guo), robert.tenzer@polyu.edu.hk (R. Tenzer), yang.ls.xu@polyu.edu.hk (Y. Xu), zhongtian.ma@connect.polyu.hk (Z. Ma).

https://doi.org/10.1016/j.apgeog.2026.103893
Received 11 September 2025; Received in revised form 5 January 2026; Accepted 6 January 2026
Available online 8 January 2026
0143-6228/© 2026 Published by Elsevier Ltd.

integrate additional park attributes, including park quality index (Xing et al., 2020), facilities completeness (Huai et al., 2023), and aesthetic features (Biernacka et al., 2022). Furthermore, as living standards and public awareness improve, visitors' subjective perceptions have gained attention as a critical dimension of accessibility. This is evidenced by the move to leverage multisource big data, such as park images, social media texts, and street view images, to quantify perceived attractiveness (Fu et al., 2024), emotional appeal (Chen et al., 2022), and overall experience (Chen, Li, et al., 2024). Such advances underscore that public perception fundamentally shapes park interactions. Indeed, the attractiveness and perceived quality of a park are not just secondary features but are central to its relaxing benefits (Kaplan, 1995) and its delivery of cultural ecosystem services (Wang et al., 2022). A park that is perceived negatively may be underutilized, rendering physical accessibility metrics misleading (Yong et al., 2023). Therefore, incorporating public perception, captured through social media sentiment or park popularity data, is a necessary step to align accessibility measurements with community experience and valuation. However, a framework that systematically integrates both online appeals and offline appeals to comprehensively profile park capacity remains underdeveloped, limiting the accuracy of park accessibility assessments.

Beyond the quality of the destination itself, the quality of the journey to the park constitutes another critical dimension of accessibility. The "ease of reach" is fundamentally shaped by micro-scale environmental features along travel routes, particularly visual greenness, which directly influences travel experience and mode choice (Wang et al., 2019). Established theories of walkability posit that journey quality is a key determinant for active travel (Ewing & Handy, 2009), a premise supported by empirical evidence showing that high Green View Index (GVI) routes provide aesthetic and psychological benefits (Ulrich et al., 1991), while visually monotonous or unsafe routes create psychological barriers that increase perceived distance (Ye et al., 2019). To quantify these route effects, conventional approaches, such as questionnaire surveys or field measurements (Cain et al., 2017; Kim et al., 2014), have provided valuable insights into pedestrian satisfaction and environmental impacts on physical activity. However, these methods are often constrained by resource demands and limited spatiotemporal coverage, making them unsuitable for city-scale analysis (Liu et al., 2023). Recent advances in Crowdsourced Geographic Information and artificial intelligence have addressed some of these limitations, enabling more efficient and scalable evaluations of street environments (Huai and Van Voorde, 2022). For instance, subsequent studies have leveraged SVIs with a diverse set of techniques, such as multi-criteria evaluation for walkability (Blečić et al., 2015), Convolutional Neural Networks (CNNs) for linking greenness to cycling frequency (Wang et al., 2020), and the Pyramid Scene Parsing Network (PSPNet) for parsing streetscape effects on walking choice (Koo et al., 2022), consistently demonstrating the value of streetscape data. Despite advances in modelling and validation, many existing studies remain confined to the dimension of spatial proximity, relying on static road networks such as OSM to infer travel behavior, often overlooking actual traffic conditions and the role of experiential quality. Furthermore, while the influence of environmental factors on active travel has been explored, comprehensive comparisons of how experiential quality differentially affects active and motorized travel within an integrated, multimodal framework remain limited.

To address these challenges in modeling travel behavior, the Two-Step Floating Catchment Area (2SFCA) method has become predominant due to its superior capacity for capturing complex supply-demand interactions (Xing et al., 2020). Specifically, 2SFCA was originally proposed as a computational framework by Radke and Mu (2000) and was later refined and formally named by Luo and Wang (2003) to better account for spatial accessibility based on supply-demand dynamics. Subsequently, Luo and Qi (2009) further advanced the method by introducing a Gaussian decay function on both supply and demand sides, leading to the Enhanced 2SFCA (E2SFCA) and stimulating extensive methodological refinement (Chen & Jia, 2019). Four key directions characterize recent improvements. One strand focuses on optimizing distance decay functions, exemplified by Gaussian (GA2SFCA) (Dai, 2010), Kernel Density (KD2SFCA) (Dai & Wang, 2011), and Empirical-Gaussian (EG2SFCA) (Kocatepe et al., 2017) approaches. Another direction extends spatial parameterization through Variable (V2SFCA) (Luo & Whippo, 2012), Dynamic (D2SFCA) (McGrail & Humphreys, 2014), and Nearest-Neighbour Modified (NN2SFCA) (Jamtsho et al., 2015) methods that enhance search radius flexibility. The third category emphasizes precise supply-demand quantification via frameworks such as the Three-Step (3SFCA) (Wan et al., 2012), Modified (M2SFCA) (Delamater, 2013), Huff model (H2SFCA) (Luo, 2014), and Optimized (O2SFCA) (Ngui & Apparicio, 2011), which introduce the competitive relationship among supply points and the choice behavior of demanders. The final improvement is integration of multimodal travel patterns, including walking, cycling and driving, to address behavioral diversity in accessibility assessments (Ni et al., 2023). While these developments have significantly enhanced the applicability of the 2SFCA method in park accessibility research, they remain confined to spatial proximity, failing to integrate experiential quality, encompassing both the park's appeal and the journey's visual greenness, into a perceptually informed accessibility measure.

Given these limited considerations, the contributions of this study are twofold. Theoretically, it proposes the concept of "greenery-perceived distance", which extends accessibility theory beyond spatial proximity by integrating experiential quality as a fundamental dimension. It also provides empirical evidence on the spatially heterogeneous role of visual greenness across travel modes and urban contexts, enriching the understanding of environmental equity. Practically, it offers urban planners a novel and replicable tool to identify and address spatial inequities in park access, considering both journey quality and destination appeal, and provides evidence-based guidance for targeted park and route improvements.

To achieve these contributions, this study developed a multimodal framework to evaluate park accessibility and equities, using Wuhan's central urban area as a case study. First, a PCA-AHP-TOPSIS approach integrates social media and POI data to derive a park attraction coefficient reflecting both online and offline appeal. Second, walking, cycling, and driving travel times, distances, and routes are obtained via the AMap Application Programming Interfaces (APIs), while route-level GVI is quantified from SVIs using PSPNet. Third, greenery-perceived distance function was calculated by integrating mobile signaling data and the gravity model, then incorporated into the 2SFCA method to assess accessibility. Finally, spatial inequalities across travel modes are analyzed using global and local Moran's I and bivariate local Moran's I.

2. Study area and data processing

2.1. Study area

Wuhan, the capital city of Hubei Province in central China, covers approximately 8569 km^2 and had a population of 12.33 million according to the seventh population census. In Recent years, Wuhan issued the Wuhan Greening Work Plan, aiming to build a distinctive "Flower City, Park City" and promote open access to urban parks and green spaces. However, due to its growing population and urban expansion, the city faces challenges related to limited green space and uneven regional park distribution. Additionally, Wuhan's complex transportation system and unique geographical layout, where the Yangtze River and Han River divide the city into three towns (Wuchang, Hankou, and Hanyang), may further impact park accessibility. Given these factors, Wuhan serves as an ideal case study for evaluating park accessibility. This research focuses on the city's main urban area, which includes the Qiaokou (QK), Jianghan (JH), Jiang'an (JA), Hanyang (HY), Wuchang (WC), Hongshan (HS), and Qingshan (QS) districts (Fig. 1(c)). To account for residents near the periphery who may use adjacent parks, urban parks within a 1 km buffer zone around these districts were also

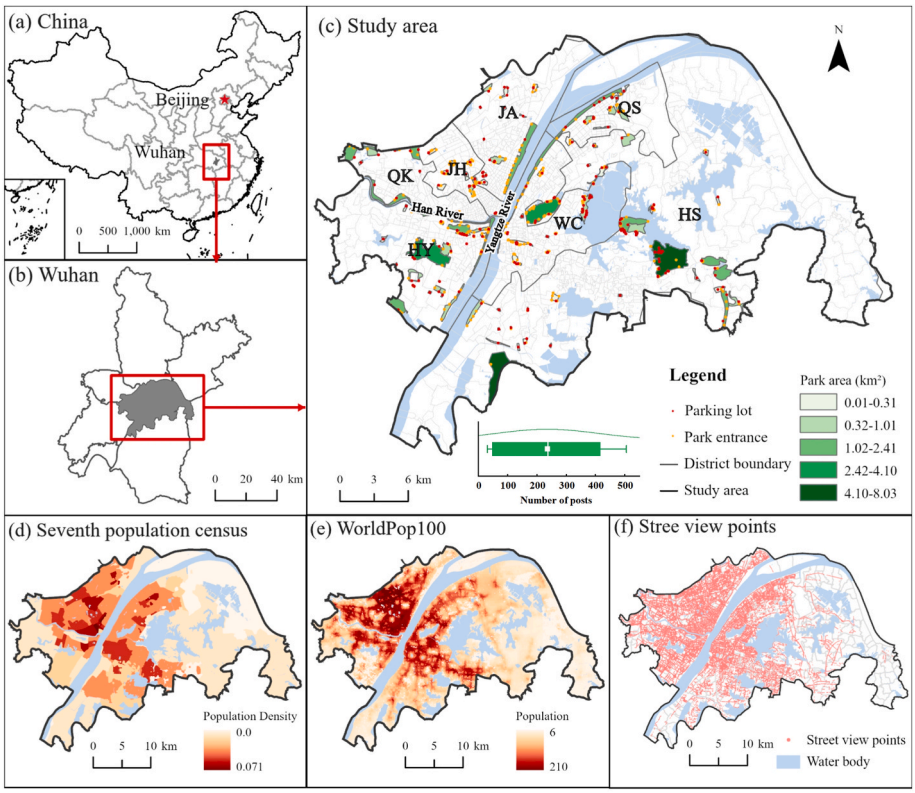

Fig. 1. Study area and main data.

included. A total of 112 urban parks, with areas ranging from 0.01 km^2 to 8.03 km^2 and an average area of 0.54 km^2, were selected as research subjects. Their spatial distribution is shown in Fig. 1(c).

2.2. Data processing

This study utilized three main data sources: population and mobility data, park and facility data, as well as evaluation and perception data.

Population and mobility data: population data at the district level for 2020 were derived from the seventh population census, including the total population, and population density was calculated by dividing area of district (Fig. 1(d)). These census data were then used to linearly correct and downscale the WorldPop100 gridded population dataset (Bondarenko et al., 2020) to the community level, following the approach of Wu and Zheng (2023), to serve as the demand measure for accessibility calculations. To assess dynamic human activity, hourly population heatmap data collected from March 11 to 17, 2019, with a search radius of approximately 250 m, was obtained through the APIs provided by the Baidu Map. The mean heat value from 7:00 a.m. to 7:00 p.m. during this period was calculated to assess park supply capacity. Mobility data provided by China Unicom (https://www.chinaunicom.com.cn/), one of the leading mobile operators in China, has a spatial resolution of approximately 250 m. It contains attributes such as date, origin-destination (OD) positions, and total population, accurately capturing human mobility patterns. To extract trips from communities to parks, all records with destinations located within parks were selected. In cases where an OD grid overlapped with multiple communities or parks, the flow value was allocated proportionally based on the overlapping area. The total number of trips from December 10 to 16, 2019, was summed to represent typical park visitation. Travel times and distances for all trips across three modes were computed using the AMap API, which revealed that 115,698, 354,503, and 507,674 trips could be made within 30 min by walking, cycling, and driving, respectively, in Wuhan's main urban area.

Park and facility data: park and facility data for 2020 were obtained from AMap. This includes the boundaries of 112 parks, 400 entrances, 327 parking lots (see Fig. 1(c)), and 3,888 facilities, with attributes such as name, location, and type. Furthermore, travel times, distances, and shortest-time routes for walking, cycling, and driving were calculated using AMap API (https://lbs.amap.com/api/webservice/guide/api/batchrequest) by constructing OD matrices. Specifically, for walking and cycling, from community centroids to park entrances, and for driving, from community centroids to park parking lots. For each OD pair, the API returned the travel time, distance, and detailed route coordinate sequences. The density of coordinates reflects actual road complexity, and denser points indicate more intricate road networks. To facilitate the calculation of the street view index, route coordinates were merged into polylines. When parks had multiple entrances, only the shortest-time route from each community was retained.

Evaluation and perception data: evaluation and perception data included Weibo texts, street view images (SVIs), and AMap travel ratings. Specifically, Weibo, a popular Chinese social media platform, was selected as our data source due to its widely recognized in park research for enabling users to freely share their experiences and comments about parks (Cheng et al., 2021). After data cleaning, 26,340 valid posts covering 112 parks were collected up to December 31, 2020, along with the number of likes, shares, and comments per post to quantify Weibo emotion and social engagement. Notably, the inclusion of the 112 parks was based on a minimum of 30 posts per park to ensure robust analysis and avoid underrepresentation (Zhao et al., 2025). The distribution of post counts across the parks is visualized in the box plot and distribution curve in Fig. 1(c). The number of posts ranges from 30 to 505, with a mean of 235 and a median of 238. The distribution of post counts is right-skewed, which aligns with the abundance of smaller parks in the study area. Additionally, the Spearman rank correlation coefficient between park area and the number of posts is 0.23, indicating a slight tendency for larger parks to generate more Weibo posts. A total of 119,421 SVIs were obtained from Baidu Maps APIs at 50-m intervals (Fig. 1

(f)). To quantify the visual greenness experienced by residents, the GVI, defined as the proportion of greenery pixels in each image, was calculated. For each travel route, the route level GVI was computed as the mean GVI value of all street view points located within a 10-m buffer of each route polyline to account for potential positioning errors. AMap travel ratings for 112 parks, derived from user visits, repeat customers, and collections, comprehensively reflect user evaluations of park quality.

3. Methods

To comprehensively evaluate park accessibility inequality, this study developed a multimodal assessment framework by integrating spatial distance and experiential quality, comprising four steps (Fig. 2). First, travel paths, times, and distances for walking, cycling, and driving were obtained from the AMap API using the OD matrix between communities and park entrances or parking lots. Second, park supply capacity was estimated by integrating the PCA-AHP-TOPSIS method with social

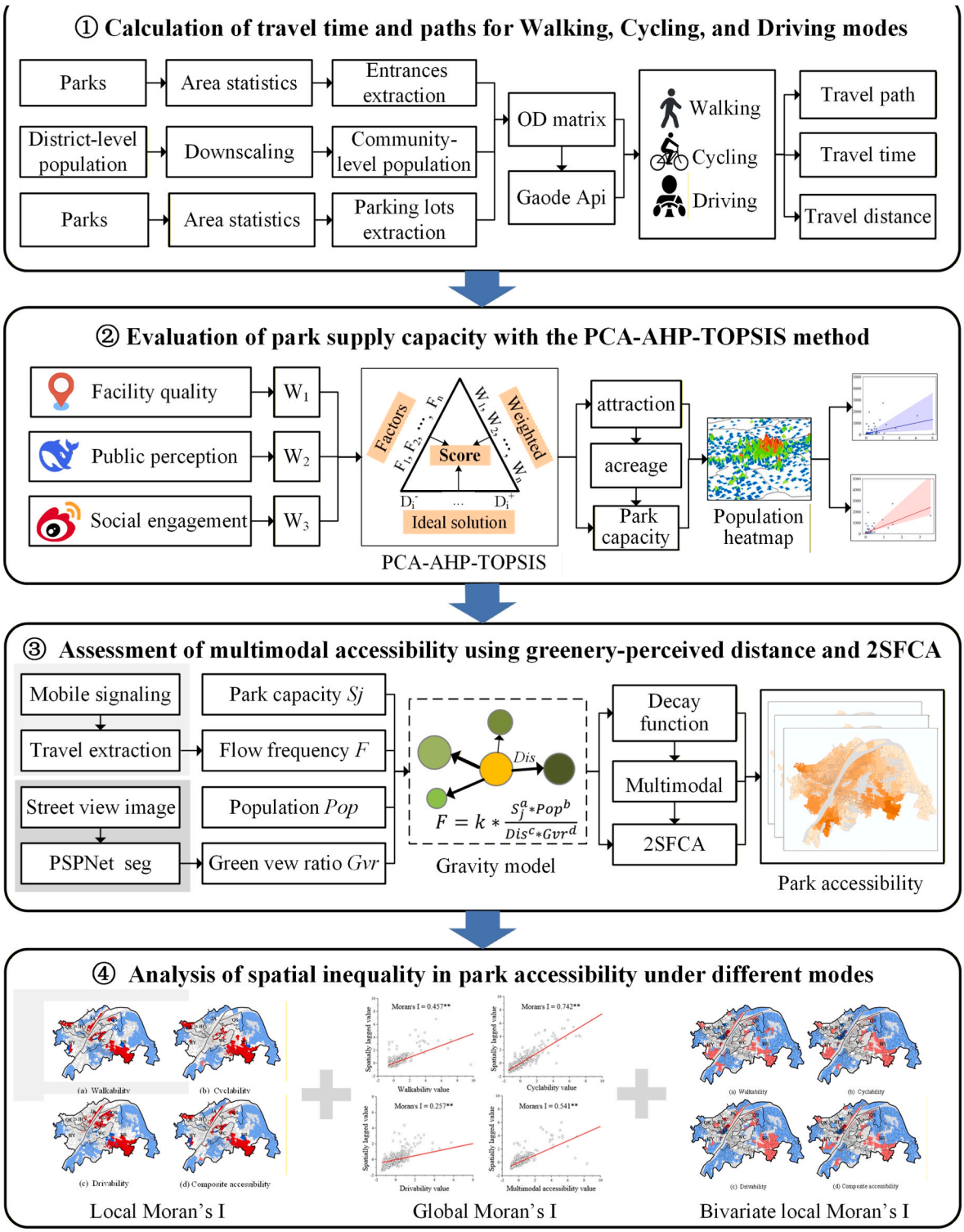

Fig. 2. Workflow of the multimodal park accessibility assessment framework.

media data. Third, multimodal accessibility was quantified by integrating the greenery-perceived distance function and the 2SFCA method, using the gravity model and mobile signaling data. Finally, global Moran's I, local Moran's I, and bivariate local Moran's I were applied to analyze spatial inequality across travel modes.

3.1. Evaluation of park supply capacity S_j with the PCA-AHP-TOPSIS method

3.1.1. Designing the attraction coefficient C_j

Evaluating park supply capacity is crucial for understanding their serve potential to surrounding communities. Traditionally, this capacity S_j has been measured by park area (Ma et al., 2025). However, public perception of park attractiveness is a complex and multi-dimensional concept that cannot be fully captured by a single type of indicator. To address this limitation, the supply catchment S_j is weighted by a composite attraction coefficient C_j. This coefficient is constructed by integrating nine indicators extracted from both online and offline sources to holistically capture the park's multi-dimensional appeal.

For online appeal, which reflects subjective public experiences and sentiments, numerous studies have demonstrated that such social media data can effectively capture public perception and collective attitudes toward urban spaces (Huang et al., 2025). Based on this, five factors were considered. First, the emotional tone of Weibo posts captures users' core experience perceptions. A total of 26,340 posts mentioning parks were classified as negative (0), positive (1), or irrelevant (2) using the DeepSeek-V3 model, a powerful and popular large language model in China (Kaygisiz & Teke, 2025). The Weibo emotion score (WES) for each park was calculated as the ratio of positive posts to the sum of positive and negative posts. To validate classification accuracy, 4000 texts were randomly sampled and manually labeled by three experts, with inconsistencies resolved through discussion. Social engagement was further quantified using Weibo likes (WLC), shares (WSC), and comments (WCC), where higher counts indicate greater popularity. Finally, AMap travel ratings (ATR) capture perceived travel and service quality; each park received ratings from over 1000 users, with scores closer to five stars indicating better experiences.

For offline appeal, which represents the objective supply capacity and physical environment, four categories of park facilities were extracted from POI data: aesthetic features count (AFC, e.g., sculptures, bridges), entertainment facilities count (EFC, e.g., tennis courts, cafes), cultural facilities count (CFC, e.g., exhibition halls, science museums), and service facilities count (SFC, e.g., restrooms, parking lots). The quantity and diversity of these facilities indicate a park's attractiveness, with higher AFC, EFC, CFC, and SFC values reflecting a greater capacity to satisfy diverse visitor needs.

By integrating both online and offline indicators, this study forms an integrated framework designed to collectively represent public perception. By bridging subjective experience and objective provision, this approach overcomes the limitations of relying on either data source alone, offering a more valid and robust measure of park attractiveness. The supply capacity S_j of park j is then calculated as:

$$S_j = S_j^a * C_j \tag{1}$$

where S_j^a is the area of park j; and C_j is the attraction coefficients derived from the 9 integrated appeal factors. The detailed calculation of C_j is provided in Section 3.1.2.

3.1.2. Calculating the attraction coefficient C_j using the PCA-AHP-TOPSIS methods

The nine factors identified in Section 3.1.1 to evaluate park attractiveness encompass both online and offline dimensions. Four offline factors (AFC, EFC, CFC, and SFC) were extracted from POI data and are widely recognized as important indicators of a park's physical attributes and facility diversity (Ma, Brindley, et al., 2025). However, these offline factors alone cannot fully capture public perception and usage. Therefore, five online factors (WES, WLC, WSC, WCC, and ATR) were incorporated to reflect real user experiences, sentiment, and engagement, which are increasingly influential in shaping the popularity and reputation of parks.

To synthesize the nine factors, the PCA-AHP-TOPSIS framework was employed to calculate the composite attraction coefficient C_j. Specifically, Principal Component Analysis (PCA) was first applied to reduce multi-collinearity by extracting independent principal components while retaining essential information (Gewers et al., 2021). Subsequently, the Analytic Hierarchy Process (AHP) was used to assign weights to these components based on expert prior knowledge, with three GIS and ecology experts performing pairwise comparisons on a 1–9 scale (Saaty, 1990). These weights were then incorporated into the TOPSIS method, where each park's relative distance to an ideal solution was computed to derive the normalized coefficient C_j, thereby avoiding subjective threshold selection (Zhang et al., 2023).

This integrated PCA-AHP-TOPSIS framework thus provides a robust, weighted ranking system that accounts for both data structure and expert-informed indicator significance (Li et al., 2021).

3.1.3. Relative contribution calculation of indicators

The calculation of the relative contribution of each original indicator to the comprehensive evaluation result was performed by tracing back through the PCA loading matrix and the AHP weights. Specifically, the contribution score (S_i) for the i-th indicator was calculated using the following equation:

$$S_i = \sum_{k=1}^{k} \lambda_k * |\omega_{ik}| \tag{2}$$

where k is the total number of principal components retained; λ_k represents the AHP weight of the k-th principal component, and ω_{ik} denotes the rotated loading of the i-th variable on the k-th principal component.

The relative contribution of each indicator i was then obtained by normalizing its contribution score against the sum of all scores:

$$\text{Relative contribution}(\%)_i = \frac{S_i}{\sum_{i=1}^{9} S_i} * 100\% \tag{3}$$

It is important to note that this contribution analysis is conducted on the integrated PCA-AHP framework. The subsequent TOPSIS method, which utilizes the weighted principal components solely for generating the final ranking, therefore does not influence the relative contribution of individual factors.

3.2. Assessment of park accessibility using greenery-perceived distance and 2SFCA

3.2.1. GVI calculation and accuracy assessment

In this study, PSPNet pretrained on the MIT ADE20K dataset (Zhou et al., 2018) was employed to segment SVIs. This choice is supported by the model's strong generalization ability and the considerable similarity in scene types and object categories between the ADE20K dataset and SVI data, indicating that the features learned from ADE20K are well-suited for our task (Fan et al., 2024; Zhang et al., 2018). Furthermore, the PSPNet model achieved a pixel wise validation accuracy across 150 categories of 81.44 % on the ADE20K dataset, demonstrating its robust performance and supporting the reliability of the segmentation results obtained in our study.

Based on segmentation results, this study calculated the GVI for each SVI from the resulting segmentation maps as the proportion of pixels assigned to greenery-related categories. The GVI_i for each street point i is defined as follows:

$$GVI_i = \frac{\sum_{i=1}^{i=n} Number\ of\ greenery\ pixel\ of\ image\ i}{\sum_{i=1}^{i=n} Number\ of\ pixel\ of\ image\ i} \tag{4}$$

where GVI_i is the greenery percentage of ith SVI; n is the number of pixels in each SVI.

To assess the accuracy of this GVI extraction process, a manual verification was performed on a randomly selected subset of 300 street view images from our dataset. The GVI for each image was visually interpreted and assigned to one of the following predefined ranges: 0–10 %, 10–20 %, 20–30 %, 30–40 %, 40–50 % and >50 %. These manual classifications served as the ground truth. The accuracy assessment results showed a strong agreement between the manual interpretation and the model outputs, with an overall classification accuracy of 83.24 % and a Cohen's Kappa coefficient of 0.81, confirming the practical reliability of our GVI data.

Furthermore, to match GVI to the three traffic modes, routes reflecting typical travel behavior were generated using the AMap API as introduced in Section 2.2. Specifically, walking and cycling routes were calculated from community centroids to park entrances, while driving routes were directed to park parking lots. This approach ensures that the routes for each mode accurately represent how residents access parks. For each mode, the AMap API provided detailed route coordinate sequences, which were merged into polylines. To account for potential positioning errors, the route level GVI was then calculated as the mean value of all street view points located within a 10-m buffer of each route polyline. The GVI for each route was calculated as follows:

$$GVI = \frac{\sum_{j=1}^{j=m} GVI_i}{m} \tag{5}$$

GVI is the mean GVI of the travel route; GVI_i is the GVI value for the ith SVI; and m is the number of SVI points located within a 10-m buffer of the travel route.

Notably, the computed route level GVI serves as our core metric for the perceptual aesthetic quality of the route environment. While infrastructural factors like traffic lights and sidewalks influence active travel, their aggregate effect on travel impedance is implicitly captured by the AMap API, which calculates paths and times based on real-world road networks and conditions. This approach allows us to isolate the independent contribution of visual greenness to park accessibility from other built-environment factors.

3.2.2. Greenery-perceived distance function extracted based on gravity model

The gravity model was selected for its unique ability to simultaneously characterize origin push forces (population size, *Pop*), destination pull forces (park supply capacity, S_j), and spatial friction (travel distance, *Dis*) (Crymble et al., 2018). Considering that GVI along travel routes may incentivize visitation, this study introduces it as a spatial gain factor and formalizes the greenery-perceived distance, a composite impedance measure that fuses physical travel distance with GVI to capture how pleasant routes feel shorter and less burdensome. Therefore, the extended gravity model in this study is represented as follows:

$$F_{ij}^{m} = k * \frac{Pop_i^a * S_j^b}{Dis_{ij}^{mc} * Gvi_{ij}^{md}} \tag{6}$$

where F_{ij}^{m} is the total visit frequency from community i to the park j within a 30 min for mode m (walking, cycling and driving), extracted from mobile signaling data; k is a constant of proportionality; Pop_i is the population of community i, obtained by downscaling district-level population data from the Seventh National Census using WorldPop100, as described in Section 2.2; S_j is the supply capacity of park j, Dis_{ij}^{mc} is the travel distance between community i and park j for mode m; Gvi_{ij}^{md} is the path-averaged GVI from the community i to park j for mode m as calculated in Section 3.2.1; and a, b, c, d are the calibrated elasticity parameters.

It is worth noting that, for the same OD pair, the AMap API may return distinct routes due to mode-specific constraints and available road infrastructure, resulting in differing travel distances and GVI values across modes. Additionally, since mobile signaling data cannot disaggregate park visit frequencies by travel mode, this study evaluated mode-specific proportions from the Fourth Wuhan Resident Travel Survey (FWRTS), conducted by Wuhan transportation research institute in 2020 (An et al., 2022). In 2020, the proportions of walking, cycling, and driving for residents in the main urban area of Wuhan were 41.5 %, 16.1 %, and 19.1 %, respectively. Therefore, in this study, these proportions were applied as follows: for any given community-park pair within a 30-min travel time by a particular mode, the proportion of trips made by that mode aligned with its overall modal proportion: walking constituted 41.5 % of the total trip volume, cycling 16.1 %, and driving 19.1 %. Therefore, the visit frequency for each mode m was estimated as:

$$F_{ij}^{m'} = \lambda^m * F_{ij}^{m} \tag{7}$$

where λ^m is the proportionality coefficient for mode m; $F_{ij}^{m'}$ is the resulting allocated frequency.

To facilitate parameter estimation, the gravity model is log-transformed, converting the original multiplicative form into a linear additive form. This transformation enables the use of Ordinary Least Squares (OLS) regression for efficient and interpretable estimation of the elasticity parameters (a, b, c, d), as well as improving model fitting and statistical inference. Therefore, equation (6) was transformed as shown below:

$$\ln\left(F_{ij}^{m'}\right) = \ln(k) + a\ln(Pop_i) + b\ln(S_j) + c\ln\left(Dis_{ij}^{m}\right) + d\ln\left(Gvi_{ij}^{m}\right) \tag{8}$$

where a, b, c, and d represent relative importance of visit frequency to population, park supply, distance, and GVI, respectively. In this log-linear form, the coefficients can be directly interpreted as elasticities, representing the percentage change in visit frequency for a 1 % change in each variable. The resulting greenery-perceived distance function is:

$$F_{(Dis,Gvr)}^{m} = Dis_{ij}^{mc} * Gvi_{ij}^{md} \tag{9}$$

where $F_{(Dis,Gvr)}^{m}$ represents the greenery-perceived distance function for mode m; c and d represent the relative importance of distance and the GVI variable for mode m. Specifically, a positive c or d indicates that greater distance or GVI corresponds to higher accessibility, while a negative value denotes the opposite.

3.2.3. Accessibility calculation using greenery-perceived distance function and 2SFCA method

The multimodal park accessibility in this study was calculated using the greenery-perceived distance function and the 2SFCA method. The method proceeds as follows:

Step1: Supply-oriented search. For each park j, search community points k within threshold t_0 setting as 30 min. The supply-demand ratio R_j^m is computed as:

$$R_j^m = \frac{S_j}{\sum\limits_{k \in \left\{ t_{kj}^m \le t_0 \right\}} P_k * F_{(Dis,Gvr)}^{m}} \tag{10}$$

where S_j represents the supply capacity of park j, as calculated in Section 3.1.2; P_k represents the population of community k, which was calculated by downscaling district-level Seventh National census data using the WorldPop100 dataset; t_{kj}^m is the travel time from community k to location j for mode m; t_0 is the threshold travel time, set to 30 min in this study. $F_{(Dis,Gvr)}^{m}$ is the greenery-perceived distance function calculated in

Section 3.2.2, which varies by transportation modes.

Step 2: Demand-oriented search. For each community i, the accessibility index is calculated by summing the supply-demand ratios R_j of the parks within the threshold travel time t_0:

$$A_i^m = \sum_{j \in \left\{ t_{ij}^m \le t_0 \right\}} R_j^m * F_{(Dis,Gvr)}^m \tag{11}$$

where A_i^m represents the accessibility of community i for mode m, and a higher value of A_i^m indicates better accessibility.

Furthermore, composite accessibility was calculated by integrating walking, cycling, and driving accessibility. Mode proportions from the FWRTS, walking (41.5 %), cycling (16.1 %), and driving (19.1 %), were normalized so their sum equals 1. Multimodal accessibility was then computed as follows:

$$A_i = 54.1\% * A_i^{walking} + 21.0\% * A_i^{cycling} + 24.9\% * A_i^{driving} \tag{11}$$

where A_i is the composite accessibility; and $A_i^{walking}$, $A_i^{cycling}$ and $A_i^{driving}$ are the accessibility values for walking, cycling, and driving modes, respectively.

3.3. Analysis of spatial inequality in park accessibility

Spatial autocorrelation measures the similarity of variable values between a location and its neighbors (Zhu et al., 2020). To evaluate global and local clustering of park accessibility across transport modes, both global and local Moran's I statistics were applied. These are computed as follows:

$$I_{global} = \frac{n \sum_{i=1}^{n} \sum_{j=1}^{n} w_{ij} (X_i - \overline{X})(X_j - \overline{X})}{\sum_{i=1}^{n} \sum_{j=1}^{n} w_{ij} \sum_{i=1}^{n} (X_i - \overline{X})^2} \tag{12}$$

$$I_{local} = \frac{(X_i - \overline{X}) \sum_{j=1}^{n} w_{ij} (X_j - \overline{X})}{S^2},$$

where

$$S^2 = \frac{\sum_{j=1, j \ne i}^{n} x_j^2}{n-1} - x^{-2} \tag{13}$$

where X_i and X_j indicate park accessibility values for community i and j, respectively; n is the total number of communities; $\overline{X}$ is the average park accessibility for the entire region; and w_{ij} represents the spatial weight matrix. The I_{global} ranges from −1 to 1: values near 1 indicate strong positive spatial autocorrelation, values near −1 signify strong negative autocorrelation, and 0 implies a random spatial pattern. The local index of spatial association (LISA) derived from I_{local} identify four cluster types: High-High and Low-Low indicate positive autocorrelations; High-Low and Low-High indicate negative autocorrelations.

Furthermore, to assess inequality and spatial mismatch between park accessibility and population density by mode, the bivariate local Moran's I statistic was used, which identifies local association patterns between two variables (Liang et al., 2023). The bivariate local Moran's I for a community x is defined as:

$$I_x = \frac{\sum_y W_{xy} Z_x Z_y}{\sum_x Z_x^2} \tag{14}$$

where Z_x represents the standardized park accessibility in community x; Z_y is the standardized population density in neighboring community y; and W_{xy} is the spatial weight defining the relationship between community x and its neighboring community y.

4. Results

4.1. Results of park supply capacity

A set of nine indicators was extracted to quantify the online and offline appeal of urban parks. Each indicator was normalized to the range [0,1], and the spatial distribution results were classified into five levels using the natural breaks method, as shown in Fig. 3. The offline appeal indicators (Fig. 3(a)–(d)) exhibit distinct patterns compared to the online appeal indicators (Fig. 3(e)–(i)). Specifically, for offline appeal, parks with high counts of aesthetic, entertainment or service facilities are relatively rare, and tend to be larger in areas. Parks with more culture facilities are typically theme parks; these parks contain a certain number of culture exhibitions but always have a small area. In contrast, the online appeal indicators display higher scores more frequently, particularly in WES and ATR. Notably, the WES scores were derived using the DeepSeek-V3 model, which achieved an overall classification accuracy of 0.86, confirming the reliability of sentiment detection. This pattern suggests that park visits often elicit positive emotions and experiences. Furthermore, the spatial distributions of WLC, WCC, and WSC are similar, and parks with high Weibo popularity are distributed across various districts and typically occupy larger areas.

Furthermore, inter-indicator relationships were examined through correlation analysis, as shown in Fig. 3 (j). Very strong positive correlations (>0.94) were observed among social engagement indicators (WLC, WCC, WSC), confirming synchronized online interactions where higher numbers of likes consistently accompanied increased comments and shares. Similarly, offline appeal-related factors (AFC, EFC, SFC) showed strong intra-group correlations, suggesting that parks with better facility provisioning generally perform well across multiple service dimensions. In contrast, cross-group correlations between offline indicators and social engagement metrics were weak (ranging from 0.24 to 0.39), and WES showed persistently low correlations with all other indicators.

To address multi-collinearity, PCA was conducted on nine indicators to reveal their underlying structure. Specifically, four principal components(PCs) were extracted, explaining 46.55 %, 20.83 %, 11.15 %, and 8.80 % of the variance in the original data, respectively, for a total of 87.32 %. Factors with loadings greater than 0.65 were selected to construct four park attraction drivers (Table 1). Specifically, PC1 (social engagement) loaded strongly on WLC, WSC, WCC; PC2 (facilities and satisfaction) captured EFC, SFC, and ATR; PC3 (cultural and aesthetic value) represented AFC and CFC; PC4 (sentiment evaluation) was defined by WES.

Furthermore, using PCA contributions as a reference, the AHP was employed to determine the relative importance of each factor via pairwise comparisons (1–9 rating scale) and expert judgment. As a result, the weights of the four PCs were determined as follows: PC1 = 0.20; PC2 = 0.56 (primary driver); PC3 = 0.09; and PC4 = 0.15.

Given that these weights are derived from expert judgment; a sensitivity analysis was conducted to evaluate the robustness of the results. Specifically, the weight of the primary component PC2 (0.56) was varied by ±10 % (0.46, 0.51, 0.61, 0.66), with the other weights proportionally redistributed to maintain a sum of 1. The park rankings under these adjusted weights showed an exceptionally high Spearman's correlation ($\rho > 0.94$) with the original ranking, confirming that the results are robust to minor variations in expert judgment.

Therefore, the weights determined through expert evaluation, were used as inputs for the TOPSIS method to evaluate park attraction and capacity. The resulting park supply capacities were then categorized into five classes, as illustrated in Fig. 4. Specifically, park supply capacity reveals a general correlation with park area. The six largest parks, situated across various districts, account for 44.8 % of the total park area and were all classified as having high or very high capacity. In contrast,

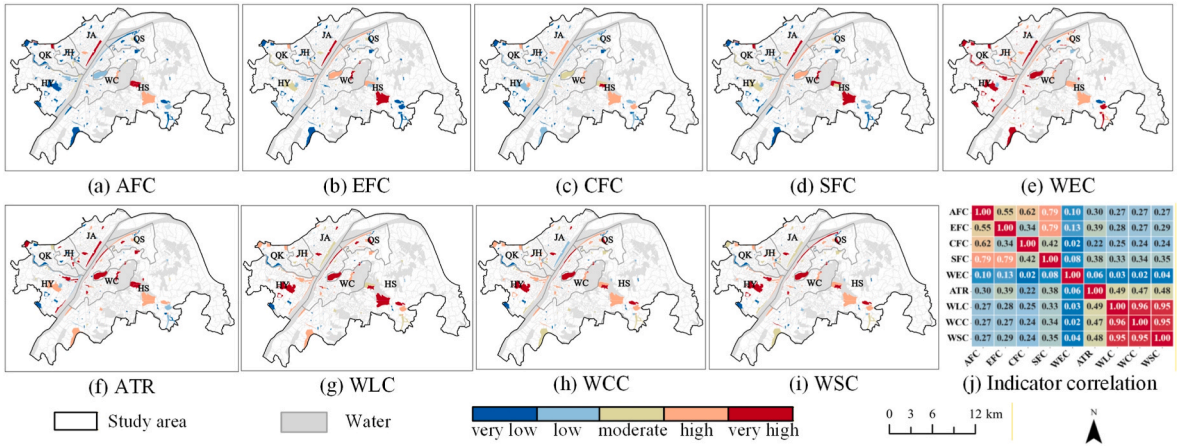

Fig. 3. Spatial distribution and correlation of the nine attractiveness indicators.

Table 1
Rotated component matrix.

Attraction indicators	Component			
	1	2	3	4
AFC	0.097	0.580	**0.703**	0.049
EFC	0.115	**0.878**	0.183	0.075
CFC	0.151	0.140	**0.902**	−0.008
SFC	0.157	**0.836**	0.392	0.020
WES	0.014	0.067	0.012	**0.997**
ATR	0.496	**0.667**	−0.111	0.007
WLC	**0.964**	0.138	0.126	0.011
WSC	**0.963**	0.137	0.124	0.001
WCC	**0.956**	0.154	0.118	0.018

over 80 % of parks are small, collectively representing only 35.2 % of the area and typically exhibiting low capacity. However, this relationship is not deterministic. Several parks, notably Ma'anshan Forest Park, Hankou Riverside Park, and Wuhan Garden Expo Park (marked as ②, ③, and ④ in Fig. 4), demonstrate a supply capacity ranking substantially higher than their area ranking. Conversely, the largest park, Huangjia Lake Wetland Park (marked as ① in Fig. 4, with only the portion within the study area displayed), exhibits limited capacity, likely due to its peripheral location and extensive water coverage, which constrain its online popularity and useable facility area.

4.2. Results of park accessibility under multimodal modes

4.2.1. GVI spatial distribution

To more clearly show the GVI's spatial distribution, the results of the SVI and spatial interpolation result are presented in Fig. 5. Fig. 5 (a) shows that 79.7 % of the street view point had GVIs below 20 %, with the highest proportions in the 0–5 % (31.27 %) and 10–20 % (26.41 %) categories. Only 7.9 % of the points exceeded 30 %, primarily along the urban periphery and near water bodies such as East Lake. Four typical street view points, two with high GVI and two with low, are marked in Fig. 5(a). It is evident that high-GVI areas typically feature dense

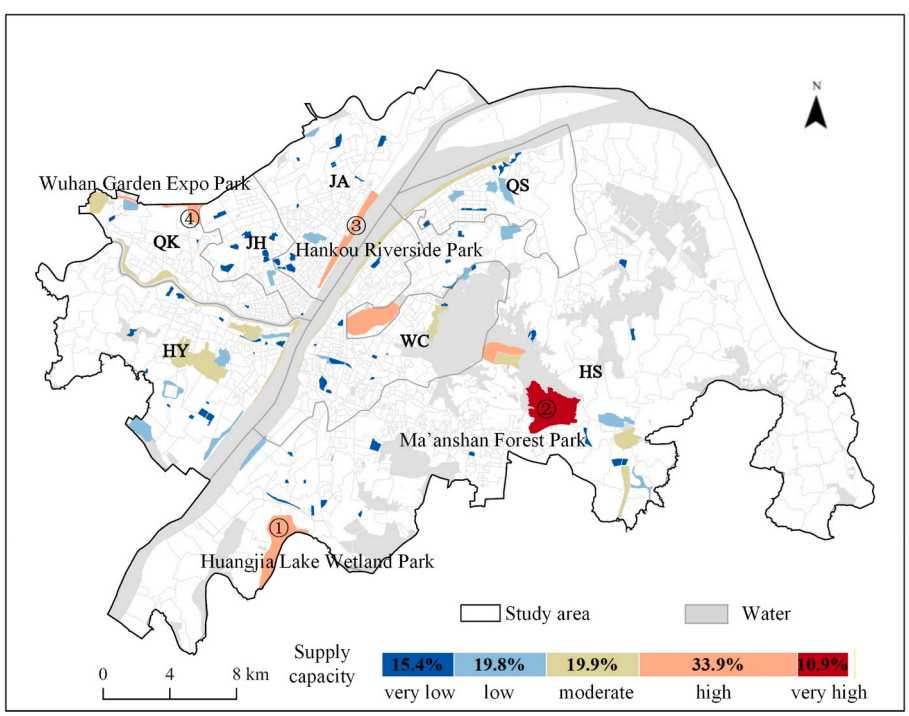

Fig. 4. Spatial distribution and areal proportion of park supply capacity.

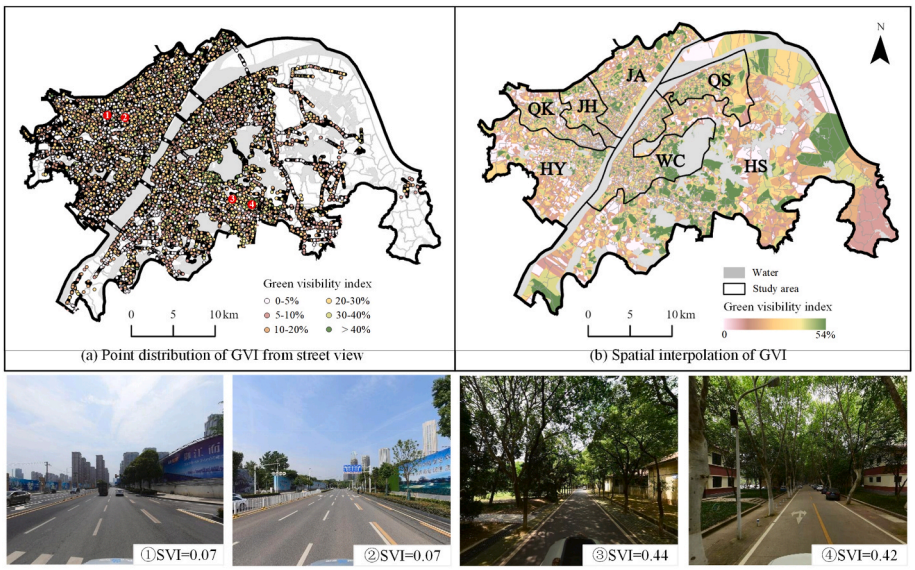

Fig. 5. Spatial distribution of GVI.

roadside trees providing substantial shade. Fig. 5(b) further illustrates the continuous distribution of GVI, revealing strong spatial heterogeneity. Central districts west of the Yangtze River (JA, JH, QK) generally show low GVI (≤20 %), while eastern districts (QS, HS) exhibit higher values, locally reaching 40 % and peaking at 54 %.

4.2.2. Greenery-perceived distance function regression results

Table 2 presents the regression results for park visitation and its determinants within a 30-min accessibility range. Variance Inflation Factors (VIFs) are all close to 1, indicating no multi-collinearity and ensuring result reliability. The R^2 and adjusted R^2 values (0.46–0.50) suggest satisfactory model fit across walking, cycling, and driving modes. Furthermore, community population (ln (Pop_i)) and park supply capacity (ln (S_j)) have significant positive effects on park visitation across all modes, with the strongest effects observed for walking (β = 0.76 and 0.84, respectively). Conversely, distance between communities i and park j (ln (Dis_{ij})) is insignificant for walking ($p = 0.96$) but exhibits significant negative effects for cycling and driving, most notably for driving ($\beta = -1.01$). Average GVI along routes (ln(Gvi_{ij})) positively influences visitation across modes, with the greatest impact for walking ($\beta = 0.62$) and the weakest for driving ($\beta = 0.04$), suggesting greener environment attract pedestrians and cyclists more than drivers.

According to equation (8) and the regression results, greenery-perceived distance functions are derived, as shown in the last line of Table 2. The results align with observed travel behavior. Within 30 min, distance minimally affects walking visitation but GVI plays a dominant positive role, whereas for cycling and especially driving, distance is the primary deterrent, where a 1 % increase in distance reduces driving visitation by approximately 1 %.

4.2.3. Park accessibility under different travel modes

Integrating greenery-perceived distance functions with the 2SFCA method, Fig. 6 illustrates pronounced spatial heterogeneity in 30-min park accessibility across walking, cycling, driving, and composite modes in Wuhan. Overall, areas along both banks of the Yangtze River and around East Lake consistently show high accessibility across all modes, coinciding with major parks such as Hankou Riverfront Park, Wuchang Riverfront Park, and East Lake Parks.

Specifically, 30-min walkability zones are mainly concentrated in central districts, while over 45.3 % of the area exhibits no access and is mainly distributed in peripheral areas. In HY, QS, and HS districts, 32.1 %, 39.1 %, and 62.4 % of the areas, respectively, lack park accessibility within 30 min. Under cycling mode, accessibility improves and expands outward, reducing the proportion of inaccessible areas to 16.4 % overall, and specifically to 6.2 %, 0 %, and 26.8 % in HY, QS, and HS, respectively. In driving mode, only HS retains one community without access, and the proportion of moderately accessible areas rises from 35.2 % (walking) to 49.8 % (cycling) and 59.5 % (driving). Composite accessibility (Fig. 6 (c)) shows a clear center-periphery gradient. Central districts and river or lake-adjacent areas exhibit very high accessibility, while peripheral regions predominantly show very low accessibility.

Interestingly, for walking and cycling, very high accessibility zones account for 17.1 % and 46.5 % in JH, 45.5 % and 12.2 % in QK, and 15.6 % and 18.9 % in HY, respectively. In contrast, driving accessibility drops sharply, with only 4.0 % in JH, 4.8 % in QK, and 0.3 % in HY. This pattern reflects the strong positive influence of surrounding greenery ($\beta = 0.62$) near Ink Lake Park, Guishan Scenic Spot and Changqing Talent Park on slow modes, contrasting with the pronounced distance decay for driving ($\alpha = -1.01$). Moreover, water detours (such as Ink Lake) and congestion-induced path penalties further limit driving accessibility,

Table 2
Regression and decay function of factors influencing park visitation across travel modes.

	Walking($R^2 = 0.50$)		Cycling($R^2 = 0.48$)		Driving($R^2 = 0.46$)	
	Coefficient	VIF	Coefficient	VIF	Coefficient	VIF
ln(Pop_i)	0.76[a]	1.00	0.53[a]	1.00	0.41[a]	1.00
ln(S_{ji})	0.84[a]	1.00	0.60[a]	1.02	0.51[a]	1.02
ln(Dis_{ij})	0.00	1.01	−0.59[a]	1.02	−1.01[a]	1.14
ln(Gvi_{ij})	0.62[a]	1.01	0.30[a]	1.03	0.04[a]	1.14
ln(k)	−13.32[a]	329.66	−5.77[a]	393.55	−0.68[a]	346.75
Greenery-perceived distance functions	$Dis_{ij}^{0}*Gvi_{ij}^{0.62}$		$Dis_{ij}^{-0.59}*Gvi_{ij}^{0.3}$		$Dis_{ij}^{-1.01}*Gvi_{ij}^{0.04}$	

[a] Correlation is significant at the 0.01 level.

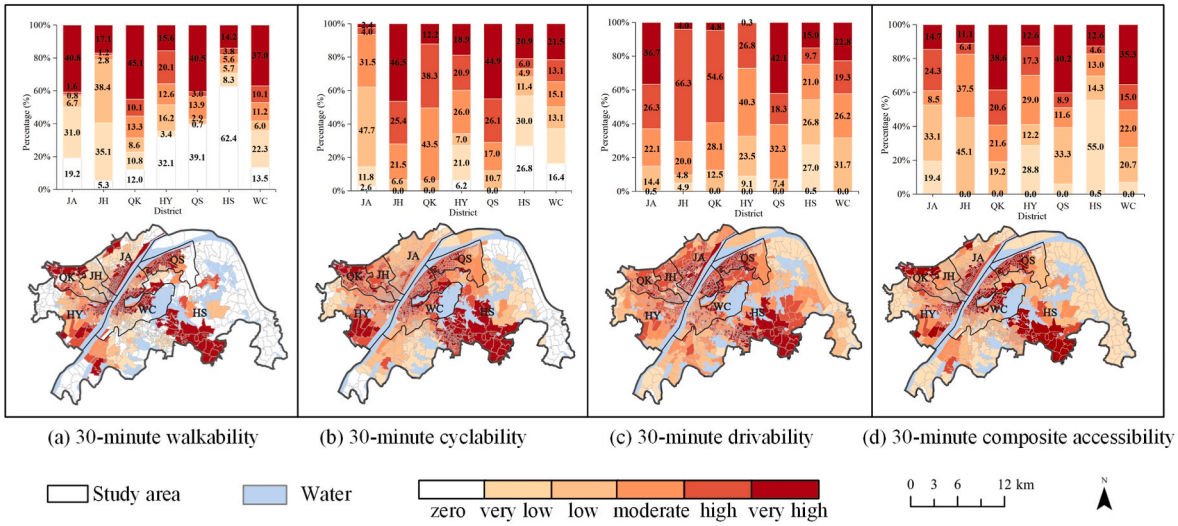

Fig. 6. Spatial distribution and area proportion of park accessibility under different travel modes.

enabling slow modes to outperform driving within 30-min coverage.

4.3. Results of park accessibility inequality

4.3.1. Spatial autocorrelation analysis of park accessibility

The global and local spatial autocorrelation results are shown in Fig. 7. Significant positive spatial autocorrelation (Global Moran's I > 0) is observed for all transport modes and composite accessibility. The Global Moran's I values are 0.457 for walking, 0.742 for cycling, 0.257 for driving, and 0.541 for composite accessibility, indicating clustered spatial patterns of park accessibility, with cycling showing the strongest clustering effect.

Complementing these global patterns, local Moran's I results reveal similar spatial clustering across all accessibility measures. High-High clusters are mainly distributed along both banks of the Yangtze River and around East Lake, while Low-Low clusters dominate outer suburban districts. High-Low and Low-High clusters are rare and occur sporadically in isolated communities.

Notable spatial disparities exist within High-High clusters. Specifically, East Lake exhibits extensive zones of high cycling accessibility, whereas the Yangtze riverfront shows more constrained clusters. This divergence is linked to site specific infrastructure and policy conditions. The cycling advantage around East Lake stems from its traffic-free 102 km greenway system (He et al., 2022), which connects multiple parks and prohibits motor vehicles, substantially enhancing cycling efficiency relative to walking. In contrast, cycling accessibility along the Yangtze riverfront is limited by access restrictions, as bicycles are prohibited from entering riverfront parks in areas such as Hankou and Wuchang.

The observed spatial clustering patterns in Fig. 7 reveal a clear dimension of accessibility inequality. Specifically, the prevalence of High-High clusters along the riverfront and around East Lake indicates that park access benefits are concentrated in these specific, often more developed and scenically advantaged areas. Conversely, the dominance of Low-Low clusters in outer suburban districts points to a systemic spatial inequality, where residents in developing outskirts are consistently deprived of adequate park services. This core-periphery divide exemplifies a geographical disparity in the distribution of public recreational resources. Moreover, the scarcity of High-Low and Low-High outliers further demonstrates that this inequality is not random, but instead reinforces the advantages of central, resource-rich zones.

4.3.2. Spatial mismatch between accessibility and population density

Fig. 8 illustrates bivariate local spatial autocorrelation patterns between park accessibility and population density across four transport

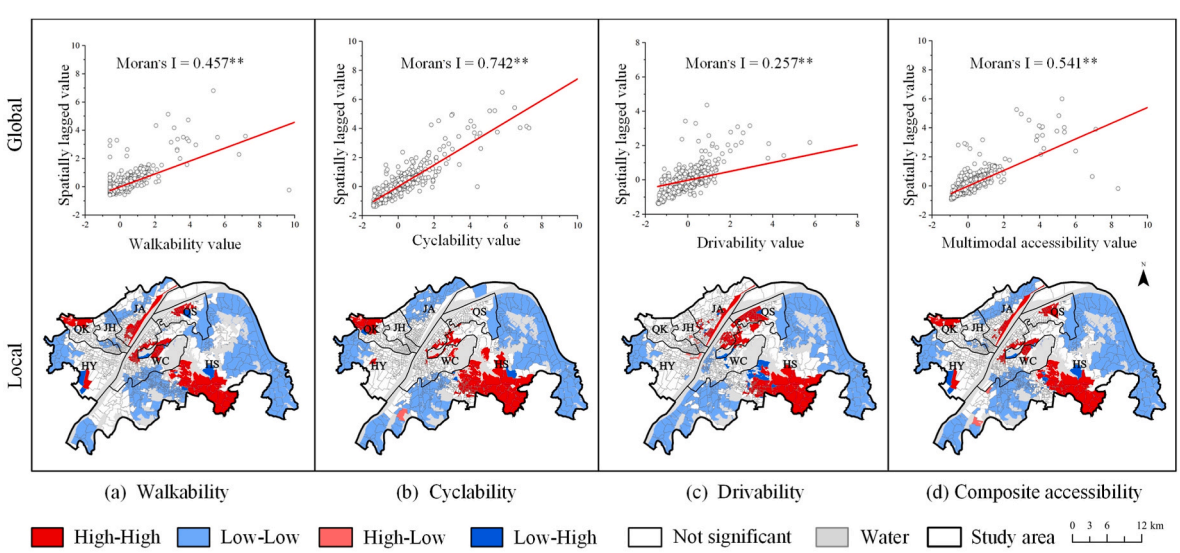

Fig. 7. Global and local spatial autocorrelation for 30-min park accessibility under multimodal modes.

modes. The results show pronounced spatial heterogeneity but consistently weak overall autocorrelation, with Moran's I values near zero (−0.012 for walking, 0.056 for cycling, 0.081 for driving, and 0.012 for composite), indicating a spatial mismatch between park accessibility and population density.

Specifically, areas showing the critical Low accessibility-High population density mismatch are limited, accounting for 0.78 % (walking), 1.13 % (cycling), 0.68 % (driving), and 0.83 % (composite). These zones are mainly located at the confluence of the Yangtze and Han Rivers, where older districts face limited park resources despite dense populations. This imbalance is most pronounced for cycling accessibility, as waterfront parks in Hankou restrict bicycles and lack integration with slow traffic networks, severely reducing service capacity in high density neighborhoods.

Conversely, areas combining high accessibility and high population density are rare, representing only 0.68 % (walking), 0.33 % (cycling), 0.78 % (driving), and 0.63 % (composite), primarily near the city center and adjacent to multiple urban parks. Their scarcity highlights a missed opportunity for equitable and efficient public service delivery.

In contrast, High accessibility–Low population density zones account for a substantial proportion: 18.11 % (walking), 19.57 % (cycling), 14.85 % (driving), and 16.60 % (composite). These are concentrated around East Lake, where extensive high-quality parks and greenways coexist with sparse populations, leading to underutilized resources and highlighting an inequitable distribution of urban green space. The concentration of premium park infrastructure in areas with low demand suggests a misallocation of public investment, disproportionately benefiting a smaller and potentially more affluent population, and thus further intensifying spatial inequality. Low accessibility-Low population density areas dominate across all modes, exceeding 50 % coverage and clustering in peripheral districts. This reflects systemic under provision of public goods in the urban periphery, which, although currently affecting fewer people, can entrench long-term inequality as these areas develop and populations grow without adequate green space planning.

5. Discussion

5.1. Enhancing park accessibility assessment by integrating supply attractiveness and greenery-perceived distance

Traditional park accessibility assessments often face two key limitations: an overreliance on simplistic supply metrics like park area, and the neglect of the experiential quality of the journey itself. This study addresses both by integrating an enhanced supply capacity measure with a greenery-perceived distance function, yielding a more realistic and equitable assessment of park accessibility.

On the supply side, this study demonstrates that park area alone inadequately represents real service capacity. By integrating offline facilities and online public feedback through a PCA-AHP-TOPSIS framework, an attraction-weighted supply capacity was constructed. Validation using Baidu heat map data shows that the attraction-weighted metric exhibits a substantially stronger correlation with observed park usage ($R^2 = 0.68$) than park area alone ($R^2 = 0.41$), indicating a more realistic representation of effective park supply (Fig. 9 (a)). Decomposition of the attraction coefficient by tracing back through the PCA loading matrix and AHP weights (Section 4.1) further reveals that recreational and service facilities (EFC and SFC) dominate supply enhancement, while online indicators, particularly attraction ratings, provide complementary insights into user satisfaction and perceived convenience (Fig. 9(b)).

Furthermore, incorporating this enhanced supply metric into the 2SFCA framework significantly mitigates the classic issue of accessibility overestimation. Compared with the traditional area-based 2SFCA, the attraction-weighted approach produces accessibility estimates that closely align with the i2SFCA method (r = 0.98) (Fig. 9 (c)), confirming its robustness and efficiency in accounting for resource competition.

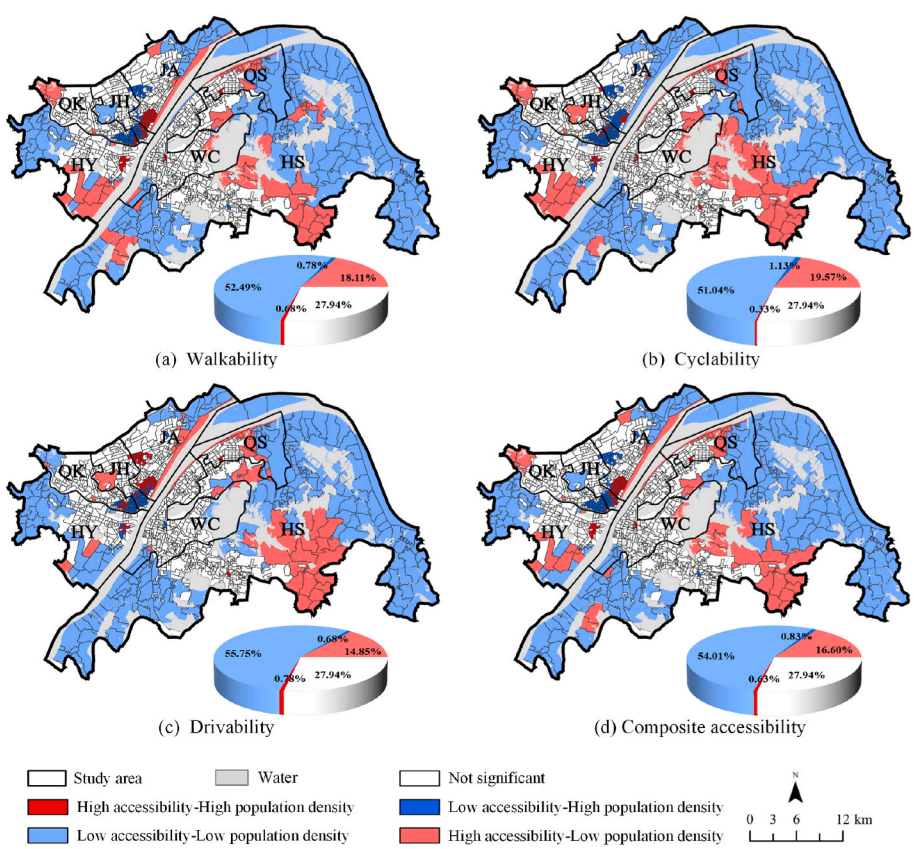

Fig. 8. Spatial mismatch between accessibility and population density.

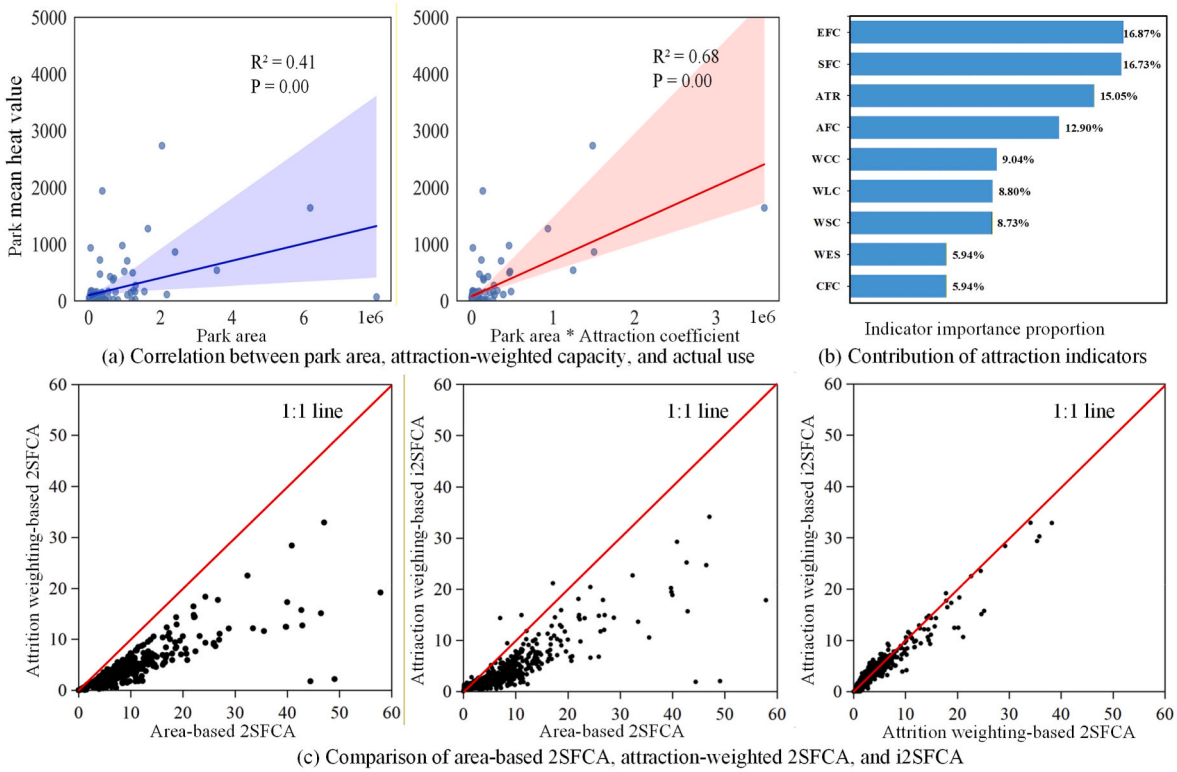

Fig. 9. Validation of attraction-weighted park supply capacity and its effect on accessibility estimation.

On the demand and travel side, the inclusion of GVI significantly improves the explanatory power of accessibility models for active travel modes. As shown in Table 3, excluding GVI reduces R^2 from 0.50 to 0.45 for walking and from 0.48 to 0.44 for cycling, while the change for driving is marginal, indicating that route greenery primarily influences non-motorized travel. Distance decay coefficients further support this pattern: walking shows a weak distance effect (−0.02), cycling exhibits a stronger decay when GVI is excluded (from −0.59 to −0.61), and driving remains dominated by distance (−1.02). These findings suggest that a substantial share of perceived impedance for walking and cycling is shaped by environmental quality rather than physical distance alone.

To further explicitly demonstrate how GVI reshapes spatial accessibility across communities, park composite accessibility was evaluated under three 2SFCA settings: a GVI-weighted model, a non-GVI model with mode-specific decay, and a traditional 1/distance model. The results indicate that omitting GVI leads to a systematic overestimation of accessibility in densely populated city centers with poor visual greenery, while accessibility near high-quality green areas is underestimated. This pattern underscores the context-dependent, marginal utility of route greenery: its perceived value and impact on accessibility are greatest in visually deprived environments.

Overall, the integration of attraction-weighted supply capacity and greenery-perceived distance functions addresses complementary shortcomings of traditional proximity-based models. By jointly accounting for park quality and travel experience, the proposed framework yields a more behaviorally realistic and equity-sensitive assessment of park accessibility, particularly for walking and cycling populations.

5.2. Validation of the robustness of the mode proportion distribution

A central methodological consideration in this study is the use of travel mode proportions from the city-wide FWRTS to represent park-specific travel patterns. To validate the use of city-wide mode shares and test model sensitivity, this study introduced a new OD dataset derived from mobile signaling data on December 13, 2019. This independent OD dataset is derived from the same mobile signaling source as the daily-resolution data introduced in Section 2.2, but features a finer temporal resolution (30-min intervals), providing a more precise benchmark for travel behavior.

First, all new OD flows within Wuhan's main urban area, including trips ending at parks, were extracted. Travel distances and times for walking, cycling, and driving were calculated via the AMap API. The analysis revealed that, for all trips across the city, 30.8 % could be completed within 30 min by walking, 69.5 % by cycling, and 91.2 % by driving. For trips specifically destined for parks, the corresponding

Table 3
Regression and decay function of gravity-based model excluding GVI.

	Walking(R^2 = 0.45)		Cycling(R^2 = 0.44)		Driving(R^2 = 0.46)	
	Coefficient	VIF	Coefficient	VIF	Coefficient	VIF
$\ln(Pop_i)$	0.75[a]	1.00	0.53[a]	1.00	0.41[a]	1.00
$\ln(S_{jj})$	0.85 [a]	1.00	0.61[a]	1.01	0.51 [a]	1.01
$\ln(Dis_{ij})$	−0.02	1.00	−0.61[a]	1.01	−1.02[a]	1.01
$\ln(k)$	−14.54[a]	301.52	−6.30[a]	357.91	−0.72[a]	336.74
Decay function	Dis_{ij}^{0}		$Dis_{ij}^{-0.61}$		$Dis_{ij}^{-1.02}$	

[a] Correlation is significant at the 0.01 level.

proportions were 27.6 %, 60.6 %, and 86.8 %, respectively. Although the absolute percentages differ, the relative patterns between modes are strongly consistent between city-wide and park-specific trips. This supports the use of city-wide mode shares as a reasonable proxy for park accessibility modeling.

Furthermore, to evaluate the sensitivity of our results to mode share sources, this study constructed an alternative scenario using proportions derived from new park-specific OD data. Based on the assumption that residents prefer lower-cost modes for short trips (walking > cycling > driving), the 30-min feasibility rates (27.6 %, 60.6 %, 86.8 %) were converted into model input proportions of 27.6 % for walking, 33.0 % for cycling, and 26.2 % for driving. The accessibility results from this scenario (Fig. 10) were compared with the original FWRTS-based findings (Fig. 6). The two result sets exhibit strong spatial concordance, supported by high Spearman rank correlations: 0.928 (walking), 0.875 (cycling), and 0.823 (driving).

Specifically, walkability patterns are highly similar; however, results based on new OD data show moderately lower values in peripheral areas (e.g., the outskirts of JA and HY districts). This may indicate a preference shift toward cycling in these locations, even for parks within a 30-min walk. Cyclability in the new OD data based results exhibits a broader spatial extent of high accessibility, extending further from the urban core. This pattern is likely attributable to the modeling assumption allocating trips near the 30-min cycling threshold to this mode, while some might be served by public transit or driving in practice. Conversely, drivability values in suburban areas are moderately lower in the new OD data scenario compared to the FWRTS-based results. This divergence is primarily due to the rational-choice logic, which reassigns a portion of potentially drivable shorter trips to walking or cycling.

Overall, despite variations in absolute values, the high spatial consistency between methods validates the FWRTS data as a reliable proxy for park accessibility patterns. Crucially, this methodological uncertainty has limited effect on the core finding: the stronger influence of GVI on active travel modes, as captured by our mode-specific greenery-perceived functions, is well supported.

5.3. Methodological contributions and policy implications

This study has developed and validated an advanced multimodal framework for assessing park accessibility. The framework offers two key methodological advances that directly inform evidence-based urban planning. First, it enhances the measurement of park supply capacity. Rather than relying solely on unidimensional metrics such as park area (Dai, 2011) or basic facility lists (Nicholls, 2001), the integrated PCA-AHP-TOPSIS method synthesizes both offline facilities and online public sentiment. This composite measure demonstrates a stronger correlation with actual park usage ($R^2 = 0.68$) compared to an area-based model ($R^2 = 0.41$), aligning with the growing recognition of multidimensional park quality (Gu et al., 2020). Furthermore, applying this coefficient within a 2SFCA model effectively mitigates the classic overestimation of accessibility, yielding results highly consistent with the more complex i2SFCA method ($r = 0.98$), as suggested by Xing et al. (2020). Second, the framework refines the representation of travel impedance by integrating the GVI into a greenery-perceived distance function. While the value of street-level greenery is acknowledged (Zhu et al., 2023), its formal incorporation into a multimodal spatial accessibility framework to uncover distributional inequities has been rare. Our results confirm GVI as a critical factor for walking and cycling, an important determinant absent in distance-only models. The observed spatial heterogeneity in accessibility, interpreted through the lens of marginal utility, provides a more realistic assessment, particularly for pedestrians and cyclists.

These methodological advancements establish a robust evidence base for rethinking urban green space policy, translating analytical insights into actionable strategies for promoting environmental equity in Wuhan and beyond. First, urban greening policy should evolve from a singular focus on park area to a multidimensional emphasis on park quality and digital engagement. The validated composite attraction coefficient provides a robust tool for prioritizing investments in both physical amenities and digital platforms, as both dimensions significantly influence visitation. Continuous monitoring of online public feedback can further enable adaptive management to meet evolving community needs. Second, the demonstrated sensitivity of walking and cycling accessibility to the GVI necessitates treating green corridors as critical infrastructure. Transportation and landscaping agencies should prioritize developing continuous, multifunctional networks over isolated interventions. This aligns with the strategic "green infrastructure" paradigm of the European Union (Angelstam et al., 2017) and the "park connector network" model of Singapore, which link green spaces to form city-wide ecological systems (Petrunoff et al., 2021). Tiered vegetation strategies, such as canopy trees along arterials and vertical greening on local streets, within 30-min walking buffers of major parks are recommended. Third, the identified spatial inequities demand targeted, context-sensitive interventions. In high density, access poor historic cores like central Hankou, planning should embrace "30-min city" principles to ensure equitable green access within a short walk or cycle (Birkenfeld et al., 2023). Tactical measures such as creating pocket parks and relaxing bicycle restrictions can offer rapid, compensatory greening. These approaches resonate with successful tactical urbanism implemented in cities like New York and Barcelona, which use low-cost installations to test and scale green interventions (Hillson, 2018; Nieuwenhuijsen et al., 2024). Finally, this integrated evaluation framework supports globally recognized sustainability and health agendas. It operationalizes the pursuit of SDGs 11.7, universal access to inclusive green space (UN, 2015). By highlighting GVI's role in promoting active travel, it also aligns with the World Health Organization's "health in all policies" principle, positioning green infrastructure as a vital public health strategy (World Health Organization, 2013). While contextualized in Wuhan, the methodological framework and policy logic offer a transferable model for fostering equitable, healthy, and

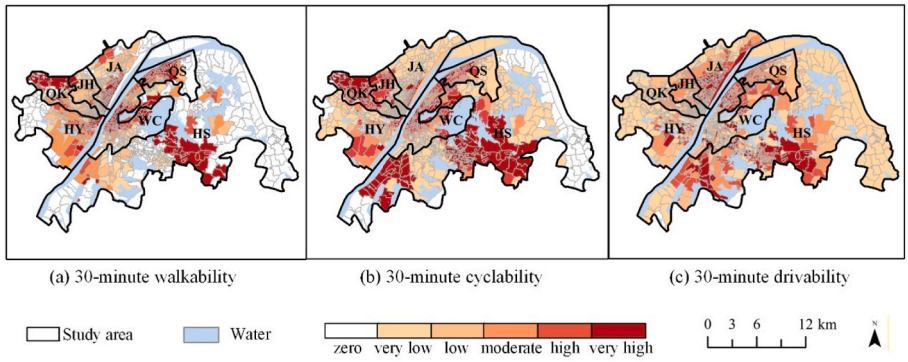

Fig. 10. Park accessibility based on 30-min resolution mobile signaling data.

sustainable urban development worldwide.

6. Conclusion

This study develops a multimodal accessibility framework for urban parks, integrating spatial proximity with experiential quality. In the case of Wuhan, results show that a PCA-AHP-TOPSIS-derived composite attraction coefficient ($R^2 = 0.68$) outperforms area-based metrics ($R^2 = 0.41$) in capturing actual use and mitigating demand overestimation. The GVI along travel routes significantly explains walking ($R^2 = 0.50$) and cycling ($R^2 = 0.48$) preferences, improving model fit and revealing pronounced spatial inequities: nearly half of walking zones (45.3 %) and a notable share of cycling zones (16.4 %) are beyond a 30-min park service threshold. These inequities are most acute in high density historic cores like Hankou, where population demand far exceeds accessible supply, while park rich areas such as East Lake show underuse, highlighting a systemic spatial inequity in park resource distribution.

Despite these improvements, this study has several limitations that point to fruitful future research directions. A key limitation is the use of city-wide travel survey data to estimate park-specific mode proportions due to data limitations, which may overlook the distinct characteristics of recreational trips. Future studies could reduce uncertainty further by exploring other purpose-specific mobility data, such as pedestrian, cycling, and vehicle trajectories, to better capture park-specific travel behavior and refine the accuracy of accessibility assessments. Secondly, this study does not incorporate sociodemographic attributes such as residents' income levels and age distribution, which future work could integrate to better account for population heterogeneity. Additionally, the route environment was characterized primarily by visual greenness. Although API derived travel times implicitly capture the aggregate effect of infrastructure on routing efficiency, the model does not explicitly parameterize the influence of specific elements such as traffic lights, sidewalks, and pedestrian crossings, or measures of the qualitative experience of safety and comfort, leaving room for subsequent studies to incorporate these detailed built environment metrics.

CRediT authorship contribution statement

Wenting Luo: Writing – original draft, Visualization, Validation, Software, Resources, Methodology, Investigation, Data curation, Conceptualization. **Yuting Guo:** Writing – original draft, Visualization, Software, Methodology, Data curation. **Robert Tenzer:** Supervision, Project administration, Funding acquisition. **Yang Xu:** Supervision, Conceptualization. **Zhongtian Ma:** Software, Formal analysis.

Funding

This work was supported by the research grant P0054667, provided by the department of the Land Surveying and Geo-Informatics at the Hong Kong Polytechnic University; and supported by the Hong Kong PhD Fellowship Scheme provided by the Research Grants Council of Hong Kong.

Declaration of competing interest

The authors declare that they have no known competing financial interests or personal relationships that could have appeared to influence the work reported in this paper.

References

An, R., Wu, Z., Tong, Z., Qin, S., Zhu, Y., & Liu, Y. (2022). How the built environment promotes public transportation in Wuhan: A multiscale geographically weighted regression analysis. *Travel Behav. Soc., 29*, 186–199. https://doi.org/10.1016/j.tbs.2022.06.011

Angelstam, P., Khaulyak, O., Yamelynets, T., Mozgeris, G., Naumov, V., Chmielewski, T. J., & Elbakidze, M. (2017). Green infrastructure development at European Union's eastern border: Effects of road infrastructure and forest habitat loss. *Journal of Environmental Management, 193*, 300–311. https://doi.org/10.1016/j.jenvman.2017.02.017

Au-Yong, C. P., Gan, X. N., Azmi, N. F., Zainol, R., & Mat Radzuan, I. S. (2023). Maintenance priority towards the features and facilities in Malaysian public parks: Visitors' perspective versus actual experience. *Ain Shams Engineering Journal, 14*(9), Article 102133. https://doi.org/10.1016/j.asej.2023.102133

Bertram, C., & Rehdanz, K. (2015). The role of urban green space for human well-being. *Ecological Economics, 120*, 139–152. https://doi.org/10.1016/j.ecolecon.2015.10.013

Biella, P., Borghesan, S., Colombo, B., Galimberti, A., Guzzetti, L., Maggioni, D., & Pioltelli, E. (2025). Lawn management promoting tall herbs, flowering species and urban park attributes enhance insect biodiversity in urban green areas. *Urban Forestry and Urban Greening, 104*, Article 128650. https://doi.org/10.1016/j.ufug.2024.128650

Biernacka, M., Łaszkiewicz, E., & Kronenberg, J. (2022). Park availability, accessibility, and attractiveness in relation to the least and most vulnerable inhabitants. *Urban Forestry and Urban Greening, 73*, Article 127585. https://doi.org/10.1016/j.ufug.2022.127585

Birkenfeld, C., Victoriano-Habit, R., Alousi-Jones, M., Soliz, A., & El-Geneidy, A. (2023). Who is living a local lifestyle? Towards a better understanding of the 15-minute-city and 30-minute-city concepts from a behavioural perspective in Montréal, Canada. *J. Urban Mobil., 3*, Article 100048. https://doi.org/10.1016/j.urbmob.2023.100048

Blečić, I., Cecchini, A., Congiu, T., Fancello, G., & Trunfio, G. A. (2015). Evaluating walkability: A capability-wise planning and design support system. *International Journal of Geographical Information Science, 29*(8), 1350–1374. https://doi.org/10.1080/13658816.2015.1026824

Bondarenko, M., Kerr, D., Sorichetta, A., & Tatem, A. *Census/projection-disaggregated gridded population datasets for 189 countries in 2020 using Built-Settlement Growth Model (BSGM) outputs*. (2020). University of Southampton. https://doi.org/10.5258/SOTON/WP00684.

Cain, K. L., Gavand, K. A., Conway, T. L., Geremia, C. M., Millstein, R. A., Frank, L. D., & Saelens, B. E. (2017). Developing and validating an abbreviated version of the microscale audit for pedestrian streetscapes (MAPS-Abbreviated). *Journal of Transport & Health, 5*, 84–96. https://doi.org/10.1016/j.jth.2017.05.004

Chen, M., Cai, Y., Guo, S., Sun, R., Song, Y., & Shen, X. (2024). Evaluating implied urban nature vitality in San Francisco: An interdisciplinary approach combining census data, street view images, and social media analysis. *Urban Forestry and Urban Greening, 95*, Article 128289. https://doi.org/10.1016/j.ufug.2024.128289

Chen, X., & Jia, P. (2019). A comparative analysis of accessibility measures by the two-step floating catchment area (2SFCA) method. *International Journal of Geographical Information Science, 33*(9), 1739–1758. https://doi.org/10.1080/13658816.2019.1591415

Chen, J., Li, H., Luo, S., Xie, J., Su, D., & Kinoshita, T. (2024). Rethinking urban park accessibility in the context of demographic change: A population structure perspective. *Urban Forestry and Urban Greening, 96*, Article 128334. https://doi.org/10.1016/j.ufug.2024.128334

Chen, S., Liu, L., Chen, C., & Haase, D. (2022). The interaction between human demand and urban greenspace supply for promoting positive emotions with sentiment analysis from Twitter. *Urban Forestry and Urban Greening, 78*, Article 127763. https://doi.org/10.1016/j.ufug.2022.127763

Cheng, Y., Zhang, J., Wei, W., & Zhao, B. (2021). Effects of urban parks on residents' expressed happiness before and during the COVID-19 pandemic. *Landscape and Urban Planning, 212*, Article 104118. https://doi.org/10.1016/j.landurbplan.2021.104118

Chiesura, A. (2004). The role of urban parks for the sustainable city. *Landscape and Urban Planning, 68*(1), 129–138. https://doi.org/10.1016/j.landurbplan.2003.08.003

Comber, A., Brunsdon, C., & Green, E. (2008). Using a GIS-based network analysis to determine urban greenspace accessibility for different ethnic and religious groups. *Landscape and Urban Planning, 86*(1), 103–114. https://doi.org/10.1016/j.landurbplan.2008.01.002

Crymble, A., Dennett, A., & Hitchcock, T. (2018). Modelling regional imbalances in English plebeian migration to late eighteenth-century london[†]. *The Economic History Review, 71*(3), 747–771. https://doi.org/10.1111/ehr.12569

Dai, D. (2010). Black residential segregation, disparities in spatial access to health care facilities, and late-stage breast cancer diagnosis in metropolitan Detroit. *Health & Place, 16*(5), 1038–1052. https://doi.org/10.1016/j.healthplace.2010.06.012

Dai, D. (2011). Racial/ethnic and socioeconomic disparities in urban green space accessibility: Where to intervene? *Landscape and Urban Planning, 102*(4), 234–244. https://doi.org/10.1016/j.landurbplan.2011.05.002

Dai, D., & Wang, F. (2011). Geographic disparities in accessibility to food stores in southwest Mississippi. *Environment and Planning B: Planning and Design, 38*(4), 659–677. https://doi.org/10.1068/b36149

Delamater, P. L. (2013). Spatial accessibility in suboptimally configured health care systems: A modified two-step floating catchment area (M2SFCA) metric. *Health & Place, 24*, 30–43. https://doi.org/10.1016/j.healthplace.2013.07.012

Doick, K. J., Peace, A., & Hutchings, T. R. (2014). The role of one large greenspace in mitigating London's nocturnal urban heat island. *Science of the Total Environment, 493*, 662–671. https://doi.org/10.1016/j.scitotenv.2014.06.048

Ewing, R., & Handy, S. (2009). Measuring the unmeasurable: Urban design qualities related to walkability. *Journal of Urban Design, 14*(1), 65–84. https://doi.org/10.1080/13574800802451155

Fan, K., Lin, A., Wu, H., & Xu, Z. (2024). Pano2Geo: An efficient and robust building height estimation model using street-view panoramas. *ISPRS Journal of Photogrammetry and Remote Sensing, 215*, 177–191. https://doi.org/10.1016/j.isprsjprs.2024.07.005

Fu, Y., Yang, J., Wang, Z., Zhang, B., Xue, J., Zeng, Y., & Li, F. (2024). Reassessing urban park accessibility: An improved two-step floating catchment area method based on the physical activity services perspective. *Urban Forestry and Urban Greening, 101*, Article 128446. https://doi.org/10.1016/j.ufug.2024.128446

Gewers, F. L., Ferreira, G. R., Arruda, H. F., Silva, F. N., Comin, C. H., Amancio, D. R., & Costa, L. D. F. (2021). Principal component analysis: A natural approach to data exploration. *ACM Computing Surveys, 54*(4), 70. https://doi.org/10.1145/3447755

Gu, X., Li, Q., & Chand, S. (2020). Factors influencing residents' access to and use of country parks in Shanghai, China. *Cities, 97*, Article 102501. https://doi.org/10.1016/j.cities.2019.102501

Hamstead, Z. A., Fisher, D., Ilieva, R. T., Wood, S. A., McPhearson, T., & Kremer, P. (2018). Geolocated social media as a rapid indicator of park visitation and equitable park access. *Computers, Environment and Urban Systems, 72*, 38–50. https://doi.org/10.1016/j.compenvurbsys.2018.01.007

He, D., Lu, Y., Xie, B., & Helbich, M. (2022). How greenway exposure reduces body weight: A natural experiment in China. *Landscape and Urban Planning, 226*, Article 104502. https://doi.org/10.1016/j.landurbplan.2022.104502

Hillson, L. (2018). Tactical Urbanism – short-term action for long-term change. *Urban Design International, 23*(1). https://doi.org/10.1057/udi.2016.9, 66–66.

Huai, S., Liu, S., Zheng, T., & Van De Voorde, T. (2023). Are social media data and survey data consistent in measuring park visitation, park satisfaction, and their influencing factors? A case study in Shanghai. *Urban Forestry and Urban Greening, 81*, Article 127869. https://doi.org/10.1016/j.ufug.2023.127869

Huai, S., & Van De Voorde, T. (2022). Which environmental features contribute to positive and negative perceptions of urban parks? A cross-cultural comparison using online reviews and Natural Language Processing methods. *Landscape and Urban Planning, 218*, Article 104307. https://doi.org/10.1016/j.landurbplan.2021.104307

Huang, W., Zhao, X., Lin, G., Wang, Z., & Chen, M. (2025). How to quantify multidimensional perception of urban parks? Integrating deep learning-based social media data analysis with questionnaire survey methods. *Urban Forestry and Urban Greening, 107*, Article 128754. https://doi.org/10.1016/j.ufug.2025.128754

Islam, A., Pattnaik, N., Moula, M. M., Rötzer, T., Pauleit, S., & Rahman, M. A. (2024). Impact of urban green spaces on air quality: A study of PM10 reduction across diverse climates. *Science of the Total Environment, 955*, Article 176770. https://doi.org/10.1016/j.scitotenv.2024.176770

Jamtsho, S., Corner, R., & Dewan, A. (2015). Spatio-temporal analysis of spatial accessibility to primary health care in Bhutan. *ISPRS International Journal of Geo-Information, 4*(3), 1584–1604. https://doi.org/10.3390/ijgi4031584

Jiang, B., He, J., Chen, J., Larsen, L., & Wang, H. (2021). Perceived green at speed: A simulated driving experiment raises new questions for attention restoration theory and stress reduction theory. *Environment and Behavior, 53*(3), 296–335. https://doi.org/10.1177/0013916520947111

Kaplan, S. (1995). The restorative benefits of nature: Toward an integrative framework. *Journal of Environmental Psychology, 15*(3), 169–182. https://doi.org/10.1016/0272-4944(95)90001-2

Kaygisiz, Ö. F., & Teke, M. T. (2025). Can deepseek and ChatGPT be used in the diagnosis of oral pathologies? *BMC Oral Health, 25*(1), 638. https://doi.org/10.1186/s12903-025-06034-x

Kim, S., Park, S., & Lee, J. S. (2014). Meso- or micro-scale? Environmental factors influencing pedestrian satisfaction. *Transportation Research Part D: Transport and Environment, 30*, 10–20. https://doi.org/10.1016/j.trd.2014.05.005

Kocatepe, A., Ulak, M. B., Ozguven, E. E., Horner, M. W., & Arghandeh, R. (2017). Socioeconomic characteristics and crash injury exposure: A case study in Florida using two-step floating catchment area method. *Applied Geography, 87*, 207–221. https://doi.org/10.1016/j.apgeog.2017.08.005

Koo, B. W., Guhathakurta, S., & Botchwey, N. (2022). How are neighborhood and street-level walkability factors associated with walking behaviors? A big data approach using street view images. *Environment and Behavior, 54*(1), 211–241. https://doi.org/10.1177/00139165211014609

Li, Y., Wu, L., Han, Q., Wang, X., Zou, T., & Fan, C. (2021). Estimation of remote sensing based ecological index along the grand canal based on PCA-AHP-TOPSIS methodology. *Ecological Indicators, 122*, Article 107214. https://doi.org/10.1016/j.ecolind.2020.107214

Liang, H., Yan, Q., Yan, Y., & Zhang, Q. (2023). Using an improved 3SFCA method to assess inequities associated with multimodal accessibility to green spaces based on mismatches between supply and demand in the metropolitan of Shanghai, China. *Sustainable Cities and Society, 91*, Article 104456. https://doi.org/10.1016/j.scs.2023.104456

Liu, W., Hu, X., Song, Z., & Yuan, X. (2023). Identifying the integrated visual characteristics of greenway landscape: A focus on human perception. *Sustainable Cities and Society, 99*, Article 104937. https://doi.org/10.1016/j.scs.2023.104937

Luo, J. (2014). Integrating the Huff model and floating catchment area methods to analyze spatial access to healthcare services. *Transactions in GIS, 18*(3), 436–448. https://doi.org/10.1111/tgis.12096

Luo, W., & Qi, Y. (2009). An enhanced two-step floating catchment area (E2SFCA) method for measuring spatial accessibility to primary care physicians. *Health & Place, 15*(4), 1100–1107. https://doi.org/10.1016/j.healthplace.2009.06.002

Luo, W., & Wang, F. (2003). Measures of spatial accessibility to health care in a gis environment: Synthesis and a case study in the Chicago region. *Environment and Planning B: Planning and Design, 30*(6), 865–884. https://doi.org/10.1068/b29120

Luo, W., & Whippo, T. (2012). Variable catchment sizes for the two-step floating catchment area (2SFCA) method. *Health & Place, 18*(4), 789–795. https://doi.org/10.1016/j.healthplace.2012.04.002

Ma, Y., Brindley, P., Wang, R., & Lange, E. (2025). Discrepancies between perceived accessibility and spatial accessibility modelling: A case study of urban parks in Guangzhou, China. *Transportation Research Part A: Policy and Practice, 191*, Article 104292. https://doi.org/10.1016/j.tra.2024.104292

Ma, G., Pellegrini, P., & Han, H. (2025). The vitality of pocket parks in high-density urban areas. An evaluation system from the users' perspective in Southwest China. *Urban Forestry and Urban Greening, 104*, Article 128596. https://doi.org/10.1016/j.ufug.2024.128596

McCormack, G. R., Rock, M., Toohey, A. M., & Hignell, D. (2010). Characteristics of urban parks associated with park use and physical activity: A review of qualitative research. *Health & Place, 16*(4), 712–726. https://doi.org/10.1016/j.healthplace.2010.03.003

McGrail, M. R., & Humphreys, J. S. (2014). Measuring spatial accessibility to primary health care services: Utilising dynamic catchment sizes. *Applied Geography, 54*, 182–188. https://doi.org/10.1016/j.apgeog.2014.08.005

Ngui, A. N., & Apparicio, P. (2011). Optimizing the two-step floating catchment area method for measuring spatial accessibility to medical clinics in Montreal. *BMC Health Services Research, 11*(1), 166. https://doi.org/10.1186/1472-6963-11-166

Ni, J., Chen, J., Fu, Z., Xi, C., & Wang, J. (2023). Examining commercial center accessibility using a modified 2SFCA method in realistic networks in Nanjing, China. *Networks and Spatial Economics, 23*(4), 1025–1045. https://doi.org/10.1007/s11067-023-09602-2

Nicholls, S. (2001a). Measuring the accessibility and equity of public parks: A case study using GIS. *Managing Leisure, 6*(4), 201–219. https://doi.org/10.1080/13606710110084651

Nieuwenhuijsen, M., De Nazelle, A., Pradas, M. C., Daher, C., Dzhambov, A. M., Echave, C., & Gössling, S. (2024). The Superblock model: A review of an innovative urban model for sustainability, liveability, health and well-being. *Environmental Research, 251*, Article 118550. https://doi.org/10.1016/j.envres.2024.118550

Petrunoff, N. A., Yi, N. X., Dickens, B., Sia, A., Koo, J., Cook, A. R., & Lin, W. H. (2021). Associations of park access, park use and physical activity in parks with wellbeing in an Asian urban environment: A cross-sectional study. *International Journal of Behavioral Nutrition and Physical Activity, 18*(1), 87. https://doi.org/10.1186/s12966-021-01147-2

Radke, J., & Mu, L. (2000). Spatial decompositions, modeling and mapping service regions to predict access to social programs. *Annals GIS, 6*(2), 105–112. https://doi.org/10.1080/10824000009480538

Saaty, T. L. (1990). *How to make a decision: The analytic hierarchy process*.

Talen, E. (1997). The social equity of urban service distribution: An exploration of park access in Pueblo, Colorado, and Macon, Georgia. *Urban Geography, 18*(6), 521–541. https://doi.org/10.2747/0272-3638.18.6.521

Ulrich, R. S., Simons, R. F., Losito, B. D., Fiorito, E., Miles, M. A., & Zelson, M. (1991). Stress recovery during exposure to natural and urban environments. *Journal of Environmental Psychology, 11*(3), 201–230. https://doi.org/10.1016/S0272-4944(05)80184-7

UN. (2015). Sustainable development goals. https://www.un.org/sustainabledevelopment/sustainable-development-goals/.

Wan, N., Zou, B., & Sternberg, T. (2012). A three-step floating catchment area method for analyzing spatial access to health services. *International Journal of Geographical Information Science, 26*(6), 1073–1089. https://doi.org/10.1080/13658816.2011.624987

Wang, R., Liu, Y., Lu, Y., Yuan, Y., Zhang, J., Liu, P., & Yao, Y. (2019). The linkage between the perception of neighbourhood and physical activity in Guangzhou, China: Using street view imagery with deep learning techniques. *International Journal of Health Geographics, 18*(1), 18. https://doi.org/10.1186/s12942-019-0182-z

Wang, R., Lu, Y., Wu, X., Liu, Y., & Yao, Y. (2020). Relationship between eye-level greenness and cycling frequency around metro stations in Shenzhen, China: A big data approach. *Sustainable Cities and Society, 59*, Article 102201. https://doi.org/10.1016/j.scs.2020.102201

Wang, Y., Shi, X., Cheng, K., Zhang, J., & Chang, Q. (2022). How do urban park features affect cultural ecosystem services: Quantified evidence for design practices. *Urban Forestry and Urban Greening, 76*, Article 127713. https://doi.org/10.1016/j.ufug.2022.127713

World Health Organization. (2013). Health in all policies: Helsinki statement. Framework for country action. https://www.who.int/publications/i/item/9789241506908.

Wu, C., Ye, X., Du, Q., & Luo, P. (2017). Spatial effects of accessibility to parks on housing prices in Shenzhen, China. *Habitat International, 63*, 45–54. https://doi.org/10.1016/j.habitatint.2017.03.010

Wu, W., & Zheng, T. (2023). Establishing a "dynamic two-step floating catchment area method" to assess the accessibility of urban green space in Shenyang based on dynamic population data and multiple modes of transportation. *Urban Forestry and Urban Greening, 82*, Article 127893. https://doi.org/10.1016/j.ufug.2023.127893

Wüstemann, H., Kalisch, D., & Kolbe, J. (2017). Access to urban green space and environmental inequalities in Germany. *Landscape and Urban Planning, 164*, 124–131. https://doi.org/10.1016/j.landurbplan.2017.04.002

Xing, L., Liu, Y., Wang, B., Wang, Y., & Liu, H. (2020). An environmental justice study on spatial access to parks for youth by using an improved 2SFCA method in Wuhan, China. *Cities, 96*, Article 102405. https://doi.org/10.1016/j.cities.2019.102405

Ye, Y., Richards, D., Lu, Y., Song, X., Zhuang, Y., Zeng, W., & Zhong, T. (2019). Measuring daily accessed street greenery: A human-scale approach for informing better urban planning practices. *Landscape and Urban Planning, 191*, Article 103434. https://doi.org/10.1016/j.landurbplan.2018.08.028

Zhang, Z., Ma, G., Lin, X., & Dai, H. (2023). Accessibility in a multiple transport mode urban park based on the "D-D" model: A case study in Park City, Chengdu. *Cities, 134*, Article 104191. https://doi.org/10.1016/j.cities.2023.104191

Zhang, F., Zhang, D., Liu, Y., & Lin, H. (2018). Representing place locales using scene elements. *Computers, Environment and Urban Systems, 71*, 153–164. https://doi.org/10.1016/j.compenvurbsys.2018.05.005

Zhao, X., Huang, H., Lin, G., & Lu, Y. (2025). Exploring temporal and spatial patterns and nonlinear driving mechanism of park perceptions: A multi-source big data study. *Sustainable Cities and Society, 119*, Article 106083. https://doi.org/10.1016/j.scs.2024.106083

Zhou, B., Zhao, H., Puig, X., Xiao, T., Fidler, S., Barriuso, A., & Torralba, A. (2018). Semantic understanding of scenes through the ADE20K dataset (No. arXiv: 1608.05442). *arXiv*. https://doi.org/10.48550/arXiv.1608.05442

Zhu, H., Nan, X., Yang, F., & Bao, Z. (2023). Utilizing the green view index to improve the urban street greenery index system: A statistical study using road patterns and vegetation structures as entry points. *Landscape and Urban Planning, 237*, Article 104780. https://doi.org/10.1016/j.landurbplan.2023.104780

Zhu, C., Zhang, X., Zhou, M., He, S., Gan, M., Yang, L., & Wang, K. (2020). Impacts of urbanization and landscape pattern on habitat quality using OLS and GWR models in Hangzhou, China. *Ecological Indicators, 117*, Article 106654. https://doi.org/10.1016/j.ecolind.2020.106654